POLITECNICO MILANO 1863

DTU Danmarks Tekniske Universitet

# Synchronized 4+4 Strokes Double Compression–Expansion Engine: One-Dimensional Simulation and Sensitivity Analysis

Extended Abstract

Davide Morerio[1]

[1] *Department of Mechanical Engineering, Politecnico di Milano, Milan, Italy*
*Advisor — Politecnico di Milano: Prof. Tommaso Lucchini*
*Advisor — Danmarks Tekniske Universitet: Prof. Bengt Håkan Johansson*

## Abstract

*This work investigates the thermodynamic potential of a synchronized Double Compression–Expansion Engine (DCEE) in a 4+4-stroke configuration, a split-cycle architecture in which compression and expansion are distributed between low-pressure (LP) and high-pressure (HP) cylinder pairs without intermediate buffer tanks. A detailed one-dimensional model was built in GT-Power and used to characterize the baseline cycle and to run a systematic parametric sensitivity study on air–fuel ratio, valve overlap, and combustion phasing. The optimized configuration reaches a brake thermal efficiency (BTE) of 48.66 %, driven by an indicated thermal efficiency of 53.92 %, at the cost of a deliberate ∼13 % reduction in brake power (104.27 to 90.7 kW). The results confirm that the synchronized DCEE 4+4 architecture can exceed conventional four-stroke efficiencies, while revealing a strong sensitivity to valve-overlap duration and combustion phasing.*

## 1. Introduction

The internal combustion engine (ICE) has remained the dominant prime mover for transportation for over a century, owing to its favourable balance of cost, power density, durability, and fuel flexibility. Yet the conventional four-stroke Otto cycle is fundamentally constrained by knock-limited compression ratios, high heat-transfer losses associated with unfavourable wall surface-to-volume ratios at top dead centre (TDC), and incomplete expansion of the combustion gases. With the transport sector responsible for roughly 18 % of global $CO_2$ emissions, and internal combustion engines expected to remain relevant in hybrid and heavy-duty applications for the foreseeable future, improving their thermodynamic efficiency beyond the conventional four-stroke limit remains a worthwhile research target.

Split-cycle architectures address this problem by decoupling the compression and expansion processes into separate cylinders, allowing each to be optimized independently. Two splitting strategies are found in the literature. *Vertical-split* engines (e.g. the Scuderi and Dolphin concepts) dedicate one cylinder bank to intake/compression and another to combustion/expansion, connected through a high-speed crossover valve; this enables independent optimization and exhaust-heat recuperation, but does not by itself reduce peak in-cylinder pressure. *Horizontal-split* engines instead divide compression and expansion themselves into two consecutive stages, reducing the pressure and temperature ratio handled by any single stage. Among horizontal-split concepts, the *Double Compression–Expansion Engine* (DCEE) splits both compression and expansion into two stages distributed across LP and HP cylinders. By reducing the geometric compression ratio required in any single cylinder while still achieving a high *overall* pressure ratio, the DCEE improves the surface-to-volume ratio at TDC — thereby reducing heat losses — and alleviates the peak-pressure constraints that limit conventional Otto-cycle efficiency. Prior simulation and experimental studies on unsynchronized DCEE variants have reported brake thermal efficiencies up to 56 %, while hydrogen-fuelled DCEE simulations have shown indicated efficiencies approaching 60 %, comparable to fuel-cell systems at full load and well above the 25–50 % BTE range typical of conventional SI/CI engines.

Two architectural choices define a given DCEE implementation: the *stroke arrangement* (2+4+2, where LP cylinders act as dedicated compressor/expander, or 4+4, where every cylinder completes a full four-stroke cycle) and the *synchronization strategy* (buffered, with intermediate storage tanks decoupling the stages, or synchronized, with direct cylinder-to-cylinder gas transfer). This work focuses specifically on the **synchronized 4+4** configuration, the most thermodynamically demanding variant because the elimination of buffer volumes requires precise valve-timing coordination between the LP and HP units to avoid additional pumping and mixing losses.

The study addresses four research questions: (i) whether the synchronized DCEE 4+4 can achieve a measurable efficiency gain over conventional four-stroke engines; (ii) how synchronization and the absence of buffer tanks affect gas-exchange losses; (iii) what trade-offs in power density and mechanical losses the architecture imposes; and (iv) how robust the optimal operating point is to variations in air–fuel ratio, valve overlap, and combustion phasing.

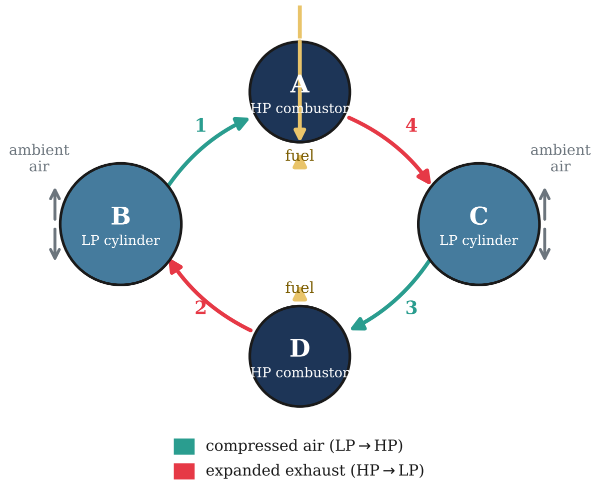


**Figure 1:** Gas-path schematic of the synchronized DCEE 4+4 architecture. Streams 1–4 indicate the timed LP↔HP gas exchange that replaces the intermediate buffer tanks of unsynchronized configurations.

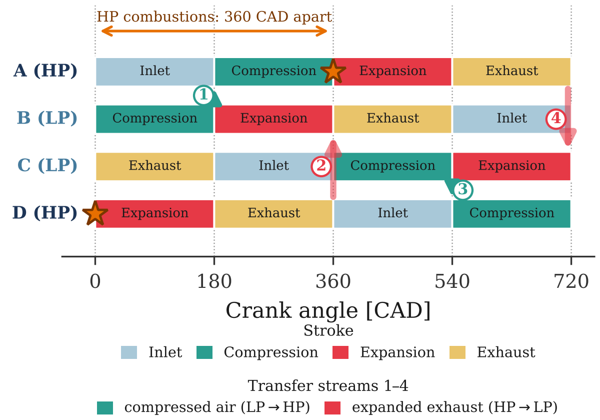


**Figure 2:** Stroke synchronization across the four cylinders over one 720° engine cycle. The two HP combustion events (stars, cylinders A and D) are phased 360° apart; the LP cylinders' second-stage expansion strokes (red) fill the intervening 180° windows, smoothing torque delivery.

## 2. Synchronized DCEE 4+4 Architecture

The investigated layout (Fig. 1) comprises two HP combustor cylinders (A, D) and two LP cylinders (B, C). Each LP cylinder performs the complete four-stroke sequence, alternating between first-stage compression of ambient air and second-stage expansion of the exhaust gases received from the HP units; consequently, the LP cylinders cannot be labelled simply as "compressor" or "expander", unlike in the 2+4+2 arrangement. The HP cylinders execute a two-stroke-equivalent sequence: intake of LP-compressed air, second-stage compression, combustion, first-stage expansion, and blow-down transfer back to the LP units. Without buffer tanks, the connecting ducts must be dimensioned so as not to behave as parasitic storage volumes, and valve timing across the four cylinders must be synchronized so that the two HP combustion events are phased 360° apart, while the intervening quarter-cycles are filled by the second-stage expansion of HP exhaust gases in the LP cylinders — yielding a torque-producing event every 180° despite only two combustion events per 720° cycle (Fig. 2).

## 3. Numerical Model

A detailed 1-D model of the synchronized DCEE 4+4 engine was developed in GT-Power (Gamma Technologies). Table 1 summarizes the cylinder geometry: the HP and LP units share the same stroke (90 mm) and rod-to-crank ratio (3.6), while bore and compression ratio differ substantially, reflecting the distinct thermodynamic roles of the two stages.

Standard sub-models were adopted for in-cylinder heat transfer (Woschni correlation), combustion (Wiebe-type heat-release law, parameterized by start of combustion and the 10–90 % mass-fraction-burned duration), fuel evaporation, and friction, in line with established 1-D engine modelling practice. The inter-cylinder connecting ducts were deliberately modelled with minimal length to approximate an idealized synchronized architecture while avoiding the introduction of significant dead volumes, and were left thermally non-insulated, allowing heat exchange with the working fluid during transfer.

**Table 1:** Cylinder geometry and kinematic parameters.

| Parameter | HP cylinder | LP cylinder |
|---|---|---|
| Bore [mm] | 75 | 150 |
| Stroke [mm] | 90 | 90 |
| Rod-to-crank ratio $l/r$ [–] | 3.6 | 3.6 |
| Compression ratio [–] | 12 | 150 |
| TDC clearance height [mm] | 0.8 | 0.5 |

Each LP cylinder is fitted with four valves (ambient intake, ambient exhaust, HP-exhaust inlet, compressed-air outlet); each HP cylinder is likewise fitted with four valves, arranged as two pairs of identical valves (2× LP-air inlet, 2× LP-transfer outlet). Valve lift, speed, acceleration and jerk profiles were derived from conventional four-stroke practice and time-shifted to enforce the inter-cylinder synchronization described in Sec. 2. The four-cylinder firing order was selected so that the two HP combustion events are phased 360° apart (Fig. 2), with the LP second-stage expansions filling the intermediate quarter-cycles; engine-component inertia and friction were modelled consistently across cylinders at a constant engine speed of 3000 rpm and standard ambient boundary conditions.

Engine performance is characterized through the Mean Effective Pressure (MEP) framework. Starting from the fuel input (FuelMEP) and the effectively released heat (QMEP),

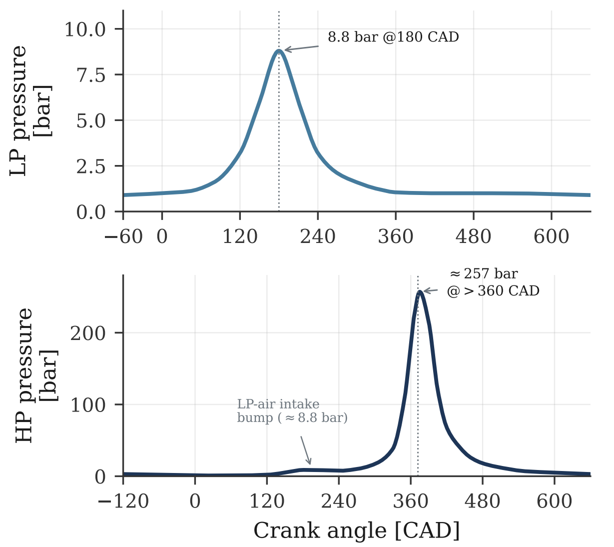


**Figure 3:** In-cylinder pressure evolution over one engine cycle for the baseline LP (top) and HP (bottom) cylinders, reconstructed from the reported GT-Power traces. Note the ∼30:1 peak-pressure ratio between stages.

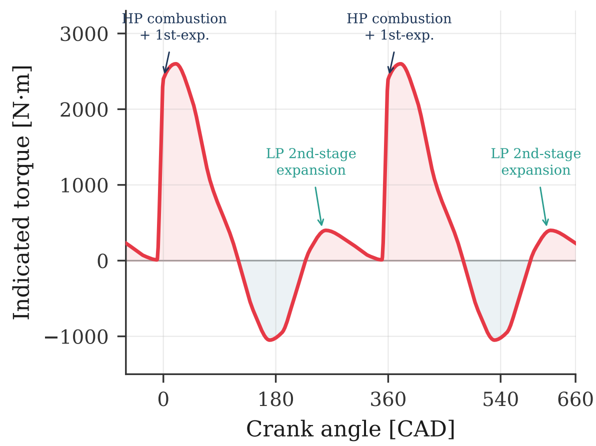


**Figure 4:** Indicated torque versus crank angle at the baseline condition, reconstructed from the reported GT-Power trace. Four peaks per cycle: two large (HP combustion + 1st-stage expansion) and two small (LP 2nd-stage expansion of residual exhaust energy).

**Table 2:** Indicated work from p–V integration (baseline).

| Quantity | Value [J] |
|---|---|
| Total net work, $W_{net,tot}$ | 4235.6 |
| Total gross work, $W_{gross,tot}$ | 4580.2 |
| Total pumping work, $W_{pump,tot}$ | −344.5 |
| Net work, HP / LP cylinder | 1619.7 / 498.1 |

the analysis separates four efficiency contributions:

$$\eta_C = \text{QMEP}/\text{FuelMEP} \quad \text{(combustion)} \tag{1}$$

$$\eta_T = \text{IMEP}_g/\text{QMEP} \quad \text{(thermodynamic)} \tag{2}$$

$$\eta_{GE} = \text{IMEP}_n/\text{IMEP}_g \quad \text{(gas exchange)} \tag{3}$$

$$\eta_M = \text{BMEP}/\text{IMEP}_n \quad \text{(mechanical)} \tag{4}$$

with the overall brake efficiency given by $\eta_B = \eta_C\,\eta_T\,\eta_{GE}\,\eta_M = \text{BMEP}/\text{FuelMEP}$. This decomposition isolates whether efficiency losses originate from incomplete combustion, thermodynamic irreversibilities, pumping work, or mechanical friction — a key analytical tool throughout the study. Because the HP and LP stages have markedly different displacements, all MEP values are reported with respect to three reference volumes (HP-only, LP-only, and total engine displacement) to avoid a biased reading of the energy distribution.

## 4. Baseline Results

At the reference operating point (3000 rpm, $\lambda = 0.83$), the LP cylinder pressure rises from ambient to a first-stage compression peak of 8.8 bar at 180 CAD, after which it decays smoothly back toward ambient as the compressed charge is transferred to the HP cylinder (Fig. 3, top). The HP trace (bottom) shows a small intermediate bump (≈8.8 bar, around 150–270 CAD) marking the admission of this LP-compressed air — matching the LP first-stage peak and confirming continuity of the thermodynamic state across the LP–HP transfer — before the second compression stage ramps the pressure up sharply to a peak of about 257 bar shortly after 360 CAD, nearly thirty times the LP peak, followed by combustion and first-stage expansion back down to a low baseline.

This 360 CAD-apart HP firing pattern is directly reflected in the indicated-torque trace (Fig. 4), which exhibits four peaks per 720 CAD cycle: two large peaks (≈2600 N m), produced by the combustion and first-stage expansion of cylinders A and D, and two smaller peaks (≈400 N m), produced as the LP cylinders extract residual thermodynamic potential from the HP exhaust gases during their second-stage expansion. Between consecutive peaks, indicated torque becomes negative (down to ≈ −1050 N m) during the compression-dominated portions of the cycle. This alternating big–small–big–small pattern is what allows the engine to deliver a torque-producing event every 180 CAD despite HP combustion occurring only every 360 CAD, smoothing the otherwise highly intermittent output of a two-HP-cylinder layout.

Numerical integration of the pressure–volume loops (Table 2) shows that the HP cylinder supplies more than three times the net work of the LP cylinder ($W_{net,HP}/W_{net,LP} = 3.25$), while pumping losses remain limited to 7.5 % of the total gross work — a relatively favourable figure for a synchronized, buffer-less architecture.

The resulting efficiency decomposition (Fig. 5) shows near-complete combustion ($\eta_C \approx 99.8\,\%$), a high thermodynamic efficiency ($\eta_T \approx 54.3\,\%$) reflecting limited heat-transfer and exhaust losses, a gas-exchange efficiency of 91.9 % despite the absence of buffer tanks, and a mechanical efficiency of 95.5 %, yielding an overall brake efficiency around 48 %. Table 3 reports the complete baseline MEP breakdown under all three reference-volume normaliza-

**Table 3:** Baseline MEP breakdown under the three reference-volume normalizations (HP-only, LP-only, total engine displacement).

| Quantity [bar] | HP-norm. | LP-norm. | Total-norm. |
|---|---|---|---|
| FuelMEP | 109.37 | 27.34 | 21.87 |
| QMEP | 109.15 | 27.28 | 21.83 |
| $\text{IMEP}_{gross}$ | 57.59 | 14.39 | 11.52 |
| $\text{IMEP}_{net}$ | 53.26 | 13.31 | 10.65 |
| PMEP | −4.33 | −1.08 | −0.87 |
| BMEP | 52.45 | 13.11 | 10.49 |
| FMEP | 0.81 | 0.20 | 0.16 |

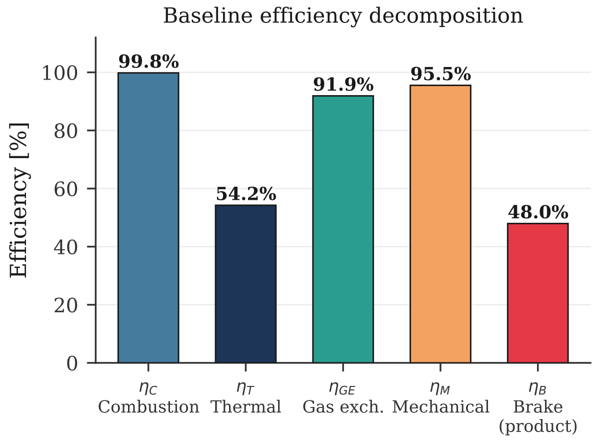


**Figure 5:** Decomposition of the baseline brake efficiency into its combustion, thermodynamic, gas-exchange, and mechanical contributions.

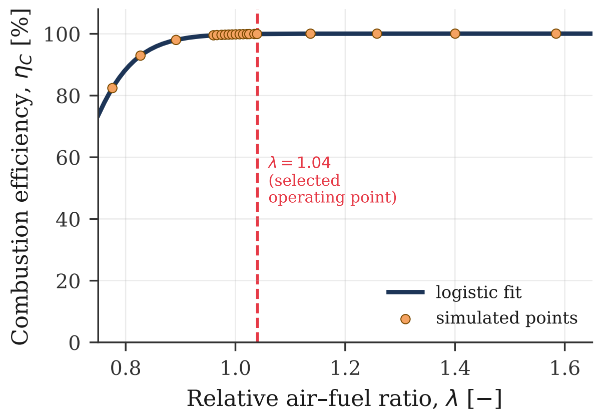


**Figure 6:** Combustion efficiency versus relative air–fuel ratio $\lambda$, with the logistic fit and the 20 simulated operating points.

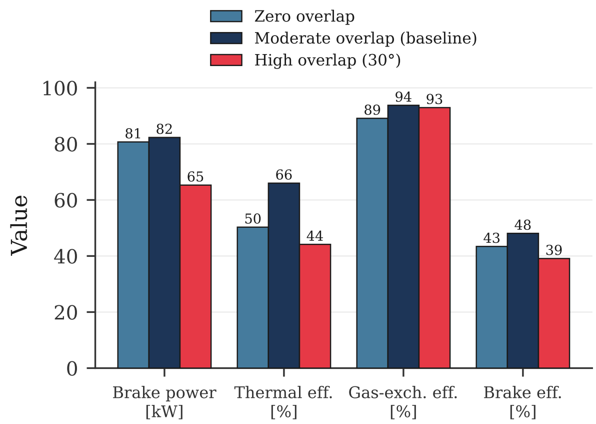


**Figure 7:** Effect of valve-overlap duration on brake power, thermal efficiency, gas-exchange efficiency, and brake efficiency.

tions; the marked dependence of the absolute MEP values on the chosen displacement is itself a direct consequence of the split-cycle nature of the architecture, and underlines why a single normalization would give an incomplete picture of the energy distribution between the HP and LP stages.

## 5. Parametric Sensitivity Analysis

### 5.1. Air–fuel ratio

Twenty simulations spanning $\lambda \approx 0.78$ to 1.58 were run to characterize the influence of mixture strength. Combustion efficiency follows a logistic transition from incomplete combustion in rich conditions to near-unity values for $\lambda \gtrsim 0.95$ (Fig. 6), fitted as $\eta_C(\lambda) = L/\left(1+e^{-k(\lambda-\lambda_0)}\right)$ with $L = 1.0006$, $k = 20.07$, $\lambda_0 = 0.699$. Thermal efficiency exhibits a local maximum at $\lambda \approx 1.04$, while gas-exchange and mechanical efficiency decrease slightly with increasing $\lambda$. The combined trade-off yields a maximum brake efficiency of 48.17 % at $\lambda = 1.04$, which was retained as the reference condition for the subsequent sensitivity studies.

### 5.2. Valve overlap

Starting from the moderate-overlap baseline ($\sim$15°, $P_b = 82.3$ kW, $\eta_B = 48.09$ %), removing the overlap entirely degrades thermal efficiency sharply (66.0 % → 50.3 %, −23.8 %) due to worsened scavenging and a higher residual gas fraction, while gas-exchange efficiency drops from 93.78 % to 89.13 %; mechanical and combustion efficiency remain essentially unaffected. Without overlap, the momentum of the exhaust gases is no longer exploited to promote inflow of the fresh charge, so residual gases dilute the incoming mixture, lowering the effective oxygen concentration and the attainable combustion temperature, and ultimately reducing peak pressure and expansion work. Conversely, an excessive overlap of 30° introduces significant short-circuiting of fresh charge directly to the exhaust port: brake power falls by 20.7 % (to 65.3 kW) and thermal efficiency drops by 33.1 % (to 44.16 %), the largest single-parameter degradation observed in the study (Fig. 7). Valve overlap therefore exhibits a markedly non-monotonic, dual-sided influence: a moderate window is essential for effective scavenging, while both insufficient and excessive overlap actively penalize efficiency through two distinct loss mechanisms (residual dilution vs. short-circuiting), making it one of the most influential and least forgiving design parameters of the synchronized architecture.

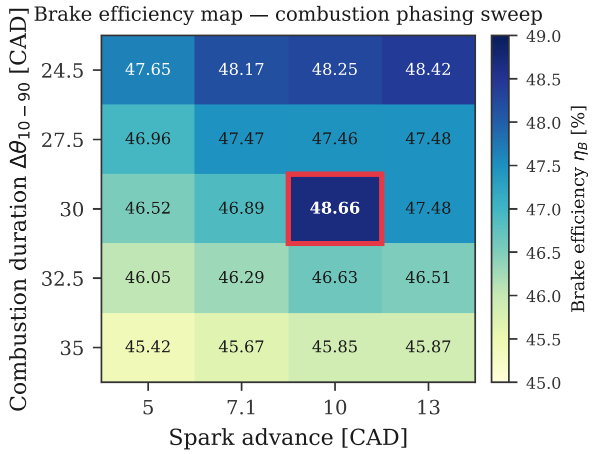


**Figure 8:** Brake efficiency as a function of combustion duration and spark advance. The global optimum (red box) defines the final operating point.

### 5.3. Combustion phasing and duration

A full factorial sweep was performed over spark advance (5, 7.1, 10, 13 CAD) and combustion duration $\Delta\theta_{10-90}$ (24.5 to 35 CAD). Combustion and mechanical efficiencies remained essentially constant across the matrix (99.8 % and ≈97.4 %, respectively), confirming that any variation in brake efficiency originates from thermodynamic phasing rather than chemical or frictional effects. Thermal efficiency decreases monotonically with longer combustion duration, as heat release increasingly deviates from the ideal constant-volume limit, and generally improves with earlier spark advance up to a point. The resulting brake-efficiency map (Fig. 8) reveals a clear global optimum at $\Delta\theta_{10-90} = 30$ CAD and spark advance of 10 CAD, yielding $\eta_B = 48.66\,\%$ and a peak indicated thermal efficiency of 53.92 %, against a minimum of 45.42 % at the longest duration and latest spark timing tested.

## 6. Discussion and Conclusions

### 6.1. Mechanistic interpretation

The torque and power reduction accompanying optimization is a direct consequence of the chosen strategy, which prioritizes thermodynamic efficiency over raw output. Efficiency-favouring operating points tend to reduce the effective in-cylinder pressure during early expansion, or to limit the overall mass flow processed per cycle, both of which lower the indicated work per cycle even as conversion efficiency improves. On the thermodynamic side, the efficiency gain is primarily linked to heat-release phasing shifted closer to TDC, increasing the effective expansion work extracted per unit of fuel; a more controlled combustion duration further reduces irreversibilities associated with late or excessively gradual heat release. These thermodynamic gains are partially offset mechanically: higher peak pressures associated with advanced phasing increase friction mean effective pressure (FMEP), so that indicated-efficiency improvements do not translate one-to-one into brake-efficiency gains. This decoupling between indicated and brake performance is a recurring and architecture-defining feature of the synchronized DCEE 4+4: improvements in one domain (thermodynamics) systematically induce penalties in another (mechanical losses, power density), confirming that the concept cannot be regarded as a drop-in evolution of the conventional engine but rather demands an integrated, multi-objective design approach.

In absolute terms, the 48.66 % brake efficiency obtained here is below the ∼56 % reported for unsynchronized DCEE variants and the ∼60 % indicated efficiency reported for hydrogen-fuelled DCEE simulations in the literature, but it was obtained under more conservative modelling assumptions (non-insulated, minimal-length ducts; no knock model; literature-derived rather than optimized valve sizing) and for a gasoline-air baseline rather than hydrogen. This positions the synchronized 4+4 result as a credible, conservative first estimate of the architecture's potential rather than an upper bound.

### 6.2. Answering the research questions

Returning to the questions posed in Sec. 1: (i) the synchronized DCEE 4+4 does achieve a measurable efficiency gain, with brake efficiency reaching 48.66 % against the 25–50 % BTE range typical of conventional four-stroke engines; (ii) the elimination of buffer tanks is shown to be viable, with gas-exchange efficiency remaining in the 92–94 % range across the sensitivity matrix, but only provided valve overlap is tightly controlled, since gas-exchange performance is highly sensitive to overlap duration; (iii) the dominant trade-off is between thermodynamic efficiency and power density, the optimized configuration trading 13 % of brake power for a 0.7-percentage-point gain in brake efficiency; and (iv) the optimum is moderately robust along the combustion-duration/spark-advance plane (within ±1 percentage point near the optimum, Fig. 8) but fragile with respect to valve overlap, where deviations of ±15° from the optimal window cost 9–19 % of brake efficiency.

Table 4 and Fig. 9 summarize the transition from the baseline to the efficiency-optimized configuration. The optimization strategy deliberately favoured thermodynamic efficiency over raw output: brake power decreased by 13 % (104.27 → 90.7 kW) and specific power density from 26.2 to 22.8 kW/L, while brake efficiency improved from ≈48.0 % to 48.66 %. At the high-pressure normalization, FuelMEP decreased by 14.2 % (109.37 → 93.87 bar) and BMEP by 13.1 % (52.45 → 45.6 bar), while pumping losses improved by 10.9 % (PMEP: −4.33 → −3.86 bar), confirming a systematic shift toward a leaner, less energy-intensive — but more efficient — operating condition.

These results confirm that the synchronized DCEE 4+4 architecture can exceed the thermal efficiency achievable by conventional four-stroke engines (typically 25–50 % BTE), while exposing the architecture's central trade-off: thermodynamic gains are only partially realized at the shaft,

**Table 4:** Baseline vs. optimized operating point.

| Parameter | Baseline | Optimized |
|---|---|---|
| Brake power [kW] | 104.27 | 90.7 |
| Brake torque [N m] | 331.92 | 288.57 |
| Indicated thermal eff. [%] | 54.25 | 53.92 |
| Brake efficiency [%] | ≈48.0 | 48.66 |
| Specific power, total [kW/L] | 26.2 | 22.8 |

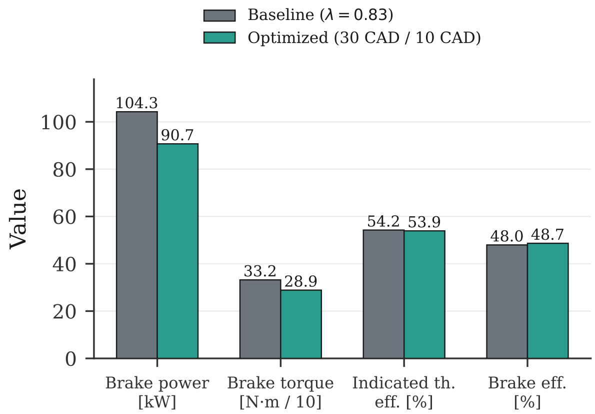


**Figure 9:** Performance and efficiency trade-off between the baseline and the efficiency-optimized configuration.

being eroded by gas-exchange and mechanical losses that are highly sensitive to valve timing. Synchronization removes the buffering effect of intermediate tanks, making the engine inherently more sensitive to timing accuracy than buffered DCEE variants.

**Limitations.** The model excludes a knock sub-model, so the reported efficiencies — particularly at advanced combustion phasing — should be regarded as theoretical upper bounds. Inter-cylinder ducts were modelled with minimal, non-physical length to approximate an idealized synchronized layout, neglecting wave-propagation and flow-inertia effects that real ducting would introduce. The combustion model is simplified, valve sizing was inherited from conventional four-stroke practice rather than optimized for the split-cycle gas path, and no experimental validation was available for this specific architecture. The 1-D framework also cannot capture three-dimensional in-cylinder flow phenomena. Finally, the analysis was restricted to a single engine speed (3000 rpm) and load point: a full speed–load operating map would be required to assess the architecture's behaviour away from the optimized design point, and its absence currently limits direct comparison with production engines characterized over standard duty cycles.

**Future work.** Priority directions include physically consistent inter-cylinder duct geometries, dedicated valve-train optimization for the split-cycle gas-exchange process, integration of a knock model to bound the achievable combustion phasing, extension of the analysis to a full speed–load operating map, and experimental validation of the synchronized 4+4 concept. Given its favourable efficiency/power-density trade-off, the architecture appears best suited to steady-state or hybrid-powertrain applications rather than high-specific-power use cases.

**Nomenclature.** *BTE*: brake thermal efficiency; *CAD*: crank angle degree; *DCEE*: Double Compression–Expansion Engine; *HP/LP*: high-/low-pressure; *TDC/BDC*: top/bottom dead centre; *MEP*: mean effective pressure; $IMEP_g$/$IMEP_n$: gross/net indicated MEP; *BMEP, FMEP, PMEP*: brake, friction, pumping MEP; $\eta_C, \eta_T, \eta_{GE}, \eta_M, \eta_B$: combustion, thermodynamic, gas-exchange, mechanical, brake efficiency; $\lambda$: relative air–fuel ratio; $\Delta\theta_{10-90}$: 10–90 % mass-fraction-burned combustion duration; *SOC*: start of combustion.

## References

[1] H. Basset, F. Finneran, "A review of split-cycle engines," *International Journal of Engine Research*, 2018, pp. 1–44.

[2] B. H. Johansson, "DCEE Short," internal presentation, 2025.

[3] R. Morgan, A. C. Salter, "Hydrogen Recuperated Advanced Thermal Engine," *Department for Energy Security & Net Zero*, UK, 2022.

[4] L. Nhut, "Double Compression-Expansion Engine concepts: experimental and simulation study of a split-cycle concept for improved brake efficiency," M.Sc. thesis, Lund University, 2019.

[5] R. Babayev, A. Andersson, H. G. Im, B. Johansson, "Hydrogen double compression–expansion engine (H2-DCEE): a sustainable internal combustion engine with 60 % thermal efficiency," *Energy Conversion and Management / Elsevier*, 2022, pp. 1–18.

[6] D. Morerio, "Synchronized 4+4 Strokes Double Compression-Expansion Engine: 1-D Simulation and Sensitivity Analysis," M.Sc. thesis, Politecnico di Milano, A.Y. 2025–2026.